3. Wakai, F., Sakaguchi, S. & Matsuno, Y. Superplasticity of yttria-stabilized tetragonal ZrO_2 polycrystals. *Adv. Ceram. Mater.* **1,** 259–263 (1986).
4. Kajihara, K., Yoshizawa, Y. & Sakuma, T. The enhancement of superplastic flow in tetragonal zirconia polycrystals with SiO_2-doping. *Acta Metall. Mater.* **43,** 1235–1242 (1995).
5. Wakai, F. *et al.* A superplastic covalent crystal composite. *Nature* **344,** 421–423 (1990).
6. Kim, B.-N., Hiraga, K., Sakka, Y. & Ahn, B.-W. A grain boundary diffusion model of dynamic grain growth during superplastic deformation. *Acta Mater.* **47,** 3433–3439 (1999).
7. Smith, C. S. Grains, phases and interfaces: an interpretation of microstructure. *Trans. Metall. Soc. AIME* **175,** 15–51 (1948).
8. Kim, B.-N., Hiraga, K., Morita, K. & Sakka, Y. Superplasticity in alumina enhanced by co-dispersion of 10% zirconia and 10% spinel particles. *Acta Mater.* **49,** 887–895 (2001).
9. McQueen, H. J. & Jonas, J. J. in *Treatise on Materials Science and Technology* Vol. 6 (ed. Arsenault, R. J.) 393–493 (Academic, New York, 1975).
10. Ting, C.-J. & Lu, H.-Y. Hot-pressing of magnesium aluminate spinel—II. microstructure development. *Acta Mater.* **47,** 831–840 (1999).
11. Morita, K. & Hiraga, K. Deformed substructures in fine-grained tetragonal zirconia. *Phil. Mag. Lett.* **81,** 311–319 (2001).
12. Schissler, D. J., Chokshi, A. H., Nieh, T. G. & Wadworth, J. Microstructural aspects of superplastic tensile deformation and cavitation failure in a fine-grained yttria stabilized tetragnal zirconia. *Acta Metall. Mater.* **39,** 3227–3236 (1991).
13. Pilling, J. & Ridley, N. Effect of hydrostatic pressure on cavitation in superplastic aluminium alloys. *Acta Mater.* **34,** 669–679 (1986).
14. Evans, A. G., Rice, J. R. & Hirth, J. P. Suppression of cavity formation in ceramics: prospects for superplasticity. *J. Am. Ceram. Soc.* **63,** 368–375 (1980).
15. Wittenauer, J. Applications of ceramic superplasticity: challenges and opportunities. *Mater. Sci. Forum* **243–245,** 653–662 (1997).

Acknowledgements

We thank N. Sekine for experimental assistance.

Correspondence and requests for materials should be addressed to B.N.K. (e-mail: KIM.Byung-Nam@nims.go.jp).

Ultrafast holographic nanopatterning of biocatalytically formed silica

Lawrence L. Brott*, Rajesh R. Naik*, David J. Pikas*, Sean M. Kirkpatrick*, David W. Tomlin*, Patrick W. Whitlock*†, Stephen J. Clarson† & Morley O. Stone*

* *Materials and Manufacturing Directorate, Air Force Research Laboratory, 3005 P Street, Wright-Patterson Air Force Base, Ohio 45433-7702, USA*
† *Department of Materials Science and Engineering, University of Cincinnati, 497 Rhodes Hall, Cincinnati, Ohio 45221-0012, USA*

Diatoms are of interest to the materials research community because of their ability to create highly complex and intricate silica structures under physiological conditions: what these single-cell organisms accomplish so elegantly in nature requires extreme laboratory conditions to duplicate[1,2]—this is true for even the simplest of structures. Following the identification of polycationic peptides from the diatom *Cylindrotheca fusiformis*, simple silica nanospheres can now be synthesized *in vitro* from silanes at nearly neutral pH and at ambient temperatures and pressures[3,4]. Here we describe a method for creating a hybrid organic/inorganic ordered nanostructure of silica spheres through the incorporation of a polycationic peptide (derived from the *C. fusiformis* silaffin-1 protein) into a polymer hologram created by two-photon-induced photopolymerization. When these peptide nanopatterned holographic structures are exposed to a silicic acid, an ordered array of silica nanospheres is deposited onto the clear polymer substrate. These structures exhibit a nearly fifty-fold increase in diffraction efficiency over a comparable polymer hologram without silica. This approach, combining the ease of processability of an organic polymer with the improved mechanical and optical properties of an inorganic material, could be of practical use for the fabrication of photonic devices.

We have recently developed a holographic two-photon-induced photopolymerization (H-TPIP) process[5] and here we describe how this technique can be used to prepare nanopatterned structures that contain biological macromolecules. Unlike conventional holograms formed through the use of ultraviolet lasers, holograms created through the two-photon process use an ultrafast infrared laser. Because infrared wavelengths typically do not alter the functionality of biological compounds, monomer formulations containing peptides can be polymerized without affecting the biological activity. We incorporated a peptide that has recently been shown to be responsible for biosilification into a formulation to be cured by a holographic two-photon-induced photopolymerization with the expectation that the peptide would be segregated into regions of low crosslinking density. The approach of using ultraviolet lasers to phase separate small liquid crystal molecules in a polymer-based hologram has been used extensively[6] and we hypothesized that this technique would also be applicable to the H-TPIP process. We predicted that exposing the peptide-containing structure to a liquid silane would cause silica to form in the holographic nanopattern (see Fig. 1) and that this hybrid organic/inorganic device would have a higher degree of order leading to a superior device compared to randomly ordered monolayers of silica on indium-tin oxide (ITO) coated glass[7].

A short 19-amino-acid R5 peptide unit (SSKKSGSYSGSKGSKRRIL) of the silaffin-1 precursor polypeptide from *C. fusiformis* is able to catalyse the formation of silica nanospheres within minutes when added to silicic acid at neutral pH and ambient temperature[3]. A chemically synthesized R5 peptide that lacks a post-translational modification of its lysine residues was used in the present work. The post-translational modification of lysine residues is required for silica formation under acidic pH conditions[3,8]. However, because our research was conducted under slightly basic conditions, the modification of the lysine residues was unnecessary. Consequently, work began by incorporating this peptide (0.80 mg in 16 μl of water) into a monomer formulation. This formulation consisted of 160 μl SR-9035, 0.022 g SR-399 (SR-9035 is a trimethylolpropane triacrylate and SR-399 is a dipentaerythritol pentaacrylate obtained from Sartomer which were used without the removal of inhibitor), 0.006 g triethanol amine and 0.005 g isopropyl thioxanthone; the entire mixture was heated for 15 min at 50 °C to aid in dissolution. The triacrylate was chosen for its high water miscibility which is due to its numerous ethylene glycol units, and the pentaacrylate was used to create a highly crosslinked system. The triethanol amine functions as a coinitiator and thioxanthone as the initiator. Typically, in a two-photon-initiated polymerization, a fluorescent chromophore is also required to absorb two photons of near-infrared laser light. The excited chromophore transfers its energy to the initiator which begins the polymerization process. However, we have found that the thioxanthone used in this formulation does not require highly coloured chromophores, and consequently, extremely large curing depths and exceptionally clear and colourless polymers are produced[9,10].

A thin layer (175 μm) of the monomer/peptide formulation was deposited onto a clean glass slide which was then placed in a miniature atmospheric chamber fitted with glass windows and

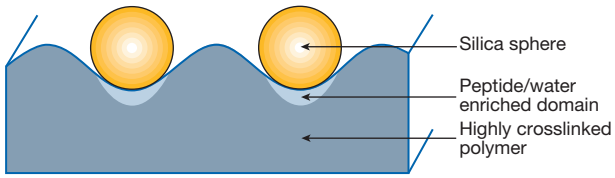

Figure 1 Cross-section of the hologram. The peptide-rich regions that are formed during the holographic polymerization process are shown.

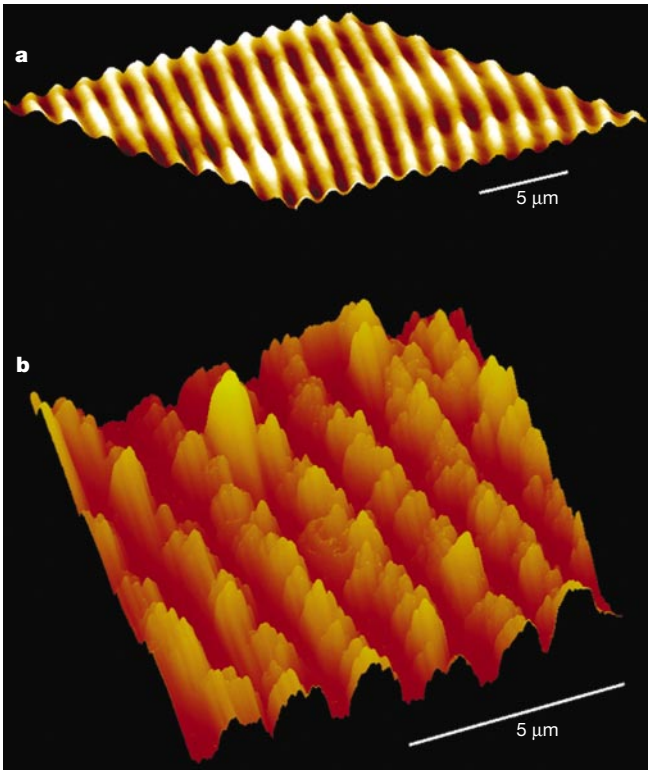

Figure 2 Surface relief pattern of the cured polymer. Atomic force microscope images of the control polymer before silification (**a**) and the hybrid structure after silification (**b**).

flushed with nitrogen. The sample was cured in a two-beam transmission holographic arrangement using a 790-nm titanium-sapphire laser (90-fs pulse width with a repetition rate of 500 Hz) for 30 s. The intensity distribution of the volume hologram drives the local polymerization rate as a function of the local field intensity, which results in alternating areas of high and low crosslink density. Because certain areas of the sample cure more rapidly than others, the smaller molecules (namely water and peptide) phase separate from the areas of higher crosslink density and migrate into areas of lower density. This phenomenon has been observed in similar systems using liquid crystals as the small molecule[6]. An alternative explanation of this phase separation could be that as the hydrophilic monomer is converted into a more hydrophobic polymer, the peptide is driven into the monomer-rich regions. As a result, peptide-rich domains are created in the polymer sample with the periodicity of the hologram. After the curing process, the sample was briefly rinsed with water to remove any uncured monomer. Atomic force microscopy (AFM) revealed that the hologram had a periodicity of 1.33 μm (see Fig. 2a).

The silane precursor (1 M tetrahydroxysilane) was synthesized by dissolving tetramethyl orthosilicate (TMOS) in 1 mM HCl. This product was then added to a sodium phosphate–citrate buffer (pH 8) to produce a final concentration of 113 mM. We note that this dilute solution remains stable for over two hours, after which it slowly converts into a clear amorphous gel. Freshly prepared hydrolysed silane was slowly applied to the hologram and allowed to react with the R5 peptide embedded in the hologram for 10 min before being rinsed with water to remove any unreacted silane. A control hologram lacking the R5 peptide was also treated with the tetrahydroxysilane solution but did not exhibit any nanosphere formation (see Fig. 3a). However, when a sample that included the peptide and was treated with the silane was analysed by scanning electron microscope, it was revealed that silica spheres formed a regular two-dimensional array with the periodicity of the hologram (see Fig. 3b). A study of the size distribution of the silica spheres reveals that the average nanosphere diameter is 452 nm (±81 nm). The silica content of the spheres was confirmed using electron dispersive spectroscopy (EDS). Additionally, analysis using the AFM indicated that the hologram had a periodicity of 1.60 μm with the silica spheres embedded in the troughs of the surface relief pattern (see Fig. 2b). The difference in the spacing between the holograms treated with and without the tetrahydroxysilane solution can be explained by the fact that the control grating shrinks as it dries out owing to water evaporation, whereas the shrinkage in the hybrid hologram is inhibited owing to the added mechanical strength of the silica spheres, preventing the ridges of the hologram from moving closer together. Consequently, the untreated grating exhibited nearly 17% more shrinkage than the treated grating. Also, the silica spheres are the most prominent feature of the hologram and the troughs in the structure are actually the peaks of the polymer.

Finally, to test the improvement that this technique can impart to an optical device, the first-order diffraction efficiency of the treated hologram was compared to that of the untreated sample. These measurements were performed by transmitting a helium-neon laser through each sample and measuring the diffraction pattern in the far field. A measurement of the incident and transmitted power in the first-order diffraction spot showed a substantial increase in the diffraction efficiency of the grating with silica versus the grating without, as would be expected from the difference in index and shrinkage. The untreated grating exhibited a diffraction efficiency of approximately 0.02%, while the grating with the silica spheres showed an efficiency of approximately 0.95%. This large increase

Table 1 Properties of holograms with and without silica nanospheres

	Hologram with silica	Hologram without silica
Grating spacing	1.60 μm	1.33 μm
Diffraction efficiency	0.95%	0.019%

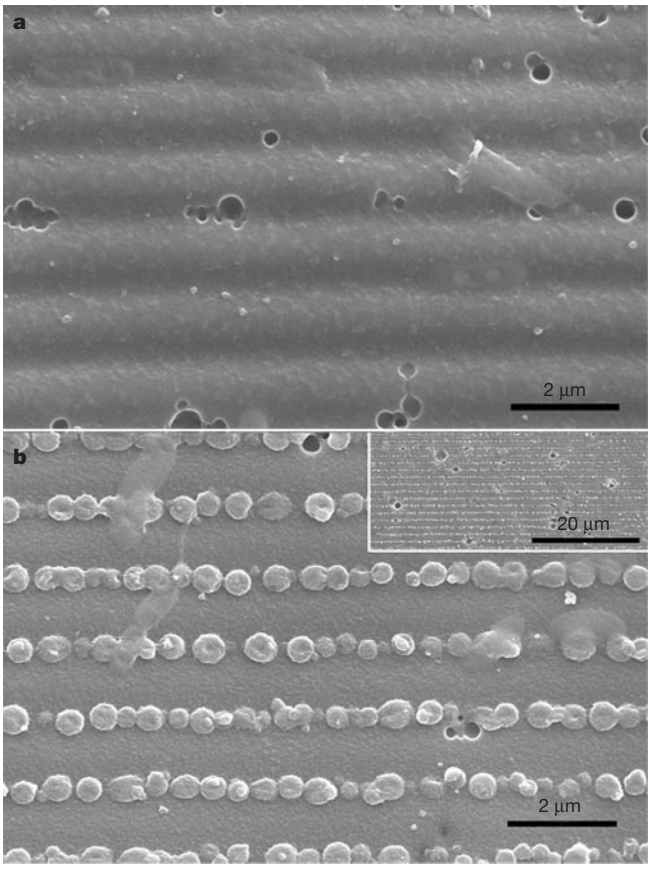

Figure 3 Two-dimensional array of ordered silica nanospheres formed within the hologram. Scanning electron microscope images of the control hologram after being treated with the liquid silane (**a**) and the biosilica nanostructure created by reacting the silane with a peptide-embedded hologram (**b**).

can be attributed to the fact that the spheres form an almost continuous line of silica along the valleys of the hologram, achieving a high fill factor. These data are summarized in Table 1.

We have thus shown that the incorporation of the peptide responsible for biosilification into a microfabricated structure using H-TPIP can result in an unusual composite organic/inorganic device that has significantly improved optical performance and superior mechanical properties compared to those of a corresponding polymeric device without silica. Although we have used a polymer/silica hybrid structure, this technique is universally applicable for any catalyst or binding agent that can be incorporated into a polymer. For example, as different catalysts are identified, a wide variety of unique hybrid structures are now possible with differing shapes and mechanical properties. Additionally, antibodies can be incorporated into the hologram and potentially used to optically identify specific antigens. Consequently, this technique allows a simple yet general and easily modifiable method for nanopatterning. □

Received 18 June; accepted 20 July 2001.

1. Parkinson, J. & Gordon, R. Beyond micromachining: the potential of diatoms. *Trends Biotechnol.* **17,** 190–196 (1999).
2. Morse, D. E. Silicon biotechnology: harnessing biological silica production to construct new materials. *Trends Biotechnol.* **17,** 230–232 (1999).
3. Kröger, N., Deutzmann, R. & Sumper, M. Polycationic peptides from diatom biosilica that direct silica nanosphere formation. *Science* **286,** 1129–1132 (1999).
4. Cha, J. N., Stucky, G. D., Morse, D. E. & Deming, T. J. Biomimetic synthesis of ordered silica structures mediated by block copolypeptides. *Nature* **403,** 289–292 (2000).
5. Kirkpatrick, S. M. *et al.* Holographic recording using two-photon-induced photopolymerization. *Appl. Phys. A* **69,** 461–464 (1999).
6. Bunning, T. J. *et al.* The morphology and performance of holographic transmission gratings recorded in polymer dispersed liquid crystals. *Polymer* **36,** 2699–2708 (1995).
7. Wang, C. *et al.* Two-dimensional ordered arrays of silica nanoparticles. *Chem. Mater.* **12,** 3662–3666 (2000).
8. Kröger, N., Deutzmann, R. & Sumper, M. Silica-precipitating peptides from diatoms, the chemical structure of silaffin-1a from *Cylindrotheca fusiformis*. *J. Biol. Chem.* **276,** 26066–26070 (2001).
9. Belfield, K. D. *et al.* Multiphoton-absorbing organic materials for microfabrication, emerging optical applications and non-destructive three-dimensional imaging. *J. Phys. Org. Chem.* **13,** 837–849 (2000).
10. Brott, L. L., Naik, R. R., Kirkpatrick, S. M., Pikas, D. J. & Stone, M. O. Near-IR two-photon induced polymerizations using either benzophenone or thioxanthone-based photoinitiators. *Polymer Preprints* **42,** 675–676 (2001).

Acknowledgements

This research was supported by the Air Force Office of Scientific Research and by funds to S.J.C. from Dayton Area Graduate Studies Institute to facilitate this UC/AFRL collaboration.

Correspondence should be addressed to M.S.
(e-mail: morley.stone@afrl.af.mil).

High-resolution record of climate stability in France during the last interglacial period

Patrick Rioual*, Valérie Andrieu-Ponel†, Miri Rietti-Shati‡, Richard W. Battarbee*, Jacques-Louis de Beaulieu†, Rachid Cheddadi†, Maurice Reille†, Helena Svobodova§ & Aldo Shemesh‡

** Environmental Change Research Centre, University College London, 26 Bedford Way, London WC1H 0AP, UK*
† Institut Méditerranéen d'Ecologie et Paléoécologie (UMR-CNRS 6116), UDESAM, Faculté des Sciences et Techniques de Saint Jérôme, 13397 Marseille Cedex 20, France
‡ Department of Environmental Sciences and Energy Research, The Weizmann Institute of Science, Rehovot 76100, Israel
§ Botanical Institute, CZ-25243 Pruhŏnice, Prague, Czech Republic

The last interglacial period (127–110 kyr ago) has been considered to be an analogue to the present interglacial period, the Holocene, which may help us to understand present climate evolution. But whereas Holocene climate has been essentially stable in Europe, variability in climate during the last interglacial period has remained unresolved, because climate reconstructions from ice cores[1,2], continental records[3,4] and marine sediment cores[5,6] give conflicting results for this period[7]. Here we present a high-resolution multi-proxy lacustrine record of climate change during the last interglacial period, based on oxygen isotopes in diatom silica, diatom assemblages and pollen–climate transfer functions from the Ribains maar in France. Contrary to a previous study[8], our data do not show a cold event interrupting the warm interglacial climate. Instead, we find an early temperature maximum with a transition to a colder climate about halfway through the sequence. The end of the interglacial period is clearly marked by an abrupt change in all proxy records. Our study confirms that in southwestern Europe the last interglacial period was a time of climatic stability and is therefore still likely to represent a useful analogue for the present climate.

In France, the sites La Grande Pile, Les Echets, Lac du Bouchet and Ribains contain continuous sedimentary records from the present to at least the penultimate glacial period (the Saalian glacial). At each site, the last interglacial (the Eemian) can be unequivocally identified[4,9,10]. At Ribains maar, the age and duration of the Eemian (local name: Ribains interglacial) has been estimated on the basis of correlation with the marine isotope stages (MISs) in